

# Developing a novel method for investigating nematode feeding behaviour using a high time-resolution phenotyping device.

Amedeo Federico Maria Leproni

Wolfson College,

Department of Chemical Engineering and Biotechnology,

Crop Science Centre,

University of Cambridge

This thesis is submitted for the degree of

Master of Philosophy, June 2024

## **Declaration**

This work was carried out at the Crop Science Centre and the Department of Chemical Engineering and Biotechnology, University of Cambridge, between October and June 2023/24.

With this statement I confirm that this thesis is the result of my own work. Any collaborations or adaptations are addressed in the text. This work is not substantially the same as any other work that has already been submitted for any degree or other qualification except as specified in the text.

This thesis does not exceed the prescribed word limit for the MPhil in Biotechnology (6,480 of 7,000 words).

# Abstract

Phenotyping nematode parasitism in plants, specifically in *Arabidopsis thaliana*, traditionally involves static timepoint observations under a microscope. This work introduces an automated imaging system that leverages machinery and computer vision to track the behaviour of *Heterodera schachtii*, the beet cyst nematode over time, focusing on its interaction with betalain-expressing *A. thaliana*, which gives roots a pink appearance. Preliminary observations indicated that nematodes acquire and metabolize betalain, visible as surface colour changes, suggesting it as a potential indicator of feeding cycles. However, existing devices' imaging frequency capability was insufficient for detailed modelling of these cycles.

We hypothesized that higher time-resolution imaging would reveal the feeding patterns of nematodes, which could ultimately inform effective control strategies against parasitism. A custom device was developed to meet specific design requirements, including high image quality, throughput, compatibility with biological methods, and robust indexing of images. The device produced over 50,000 images across 14 axenic-culture dishes over three weeks and demonstrated the feasibility of tracking nematode colour changes indicative of feeding behaviour.

Results showed that while the device could detect changes in nematode coloration, the anticipated cyclic feeding patterns were not observed. This discrepancy may be attributed to differences in *A. thaliana* lines, stress from the experimental setup, or disruption from the imaging conditions. Despite this, the work highlights the device's potential for capturing high resolution temporal data of nematode behaviour, suggesting avenues for future research use, and potential disruption mechanisms of nematode feeding cycles to enhance parasitism control methods.

## Acknowledgements

I would like to thank Dr. Olaf Kranse for his diligent help and support through this project, for always being there to help and encourage me when things were challenging. I would like to thank Prof. Sebastian Eves-van den Akker for giving me the opportunity to carry out my MPhil thesis under his wise guidance and clear vision. During this project I have come to discover how a passionate and competent scientist acts, and I have learnt skills that will serve me all my life.

Mamman, Papà, aucun fils ne pourrait demander plus que ce que vous continuez de me donner. Rien de tout cela ne serait possible sans votre soutien et votre amour. Ugi, Caro, vous êtes toujours des exemples de douceur et de gentillesse. Nonna Germana, nonna Rita, nonno Roberto, i miei cari zii e cugini grazie di accogliermi e prestare sempre i vostri saggi consigli. Adorámus Te, Christe, et benedícimus te; Quia per sanctam Crucem tuam redemísti mundum.

Many thanks also to Dr. Raquel Costa for helping me to find the path through this Biotechnology MPhil, and to the many others who have supported me. Beth, Elliot, Estefany, Javiera, Josh, Lawrence, Ollie, and Priya, for their precious help in the workshop and in the lab.

## Table of Contents

Abstract .....	3
List of Abbreviations.....	8
Chapter 1 - Introduction.....	9
Plant parasitic nematodes (PPNs) .....	9
Control measures.....	9
Lifecycle of <i>Heterodera schachtii</i> .....	10
Observation and hypothesis.....	11
Preliminary observation .....	11
Hypothesis and investigative rationale.....	13
Chapter 2 - Literature review .....	14
Feeding behaviour.....	14
Imaging limitations.....	15
Chapter 3 - Materials and methods .....	17
Biological methods .....	17
Axenic culture of <i>Heterodera schachtii</i> on <i>Arabidopsis thaliana</i> .....	17
Engineering methods .....	17
Introduction to engineering methods.....	17
Design requirements .....	18
Hardware design rationale and implementation .....	19
Fabrication methods.....	21
Logic flow diagrams.....	22
Image processing pipeline.....	23
Chapter 4 - Results .....	24
Device performance .....	24
Mechanism for tracking colour change .....	25
Observed feeding behaviour.....	27
Chapter 5 - Discussion .....	29
Device performance evaluation.....	29
Proposed design modifications.....	29

Device applicability .....	30
Experimental evaluation.....	31
Experimental failures.....	31
Disruption of feeding cycles.....	32
Uncoloured nematodes.....	32
Chapter 6 – Conclusion.....	33
References.....	34
Appendices .....	37
Appendix - Engineering methods .....	37
3D CAD design .....	37
Bill of materials.....	37
I2C interface.....	37
Circuit diagram and PCB design.....	37
Device Python script .....	37
Appendix – data analysis .....	37
Image processing Python script.....	37
RGB colour space.....	37

## Table of Figures

Figure 1: From left to right, top then bottom, the growth and variation in pink colour of a nematode over 8 days.....	12
Figure 2: Over and underfitting of data with low time-resolution. Y-axis = presence of pink. X-axis = sample number. Every sample represents the colour observed for a given image capture, over a timespan of 8 days.....	12
Figure 3: Duration of feeding phases of female <i>H. schachtii</i> adapted from Wyss and Grundler <sup>23</sup> .....	15
Figure 4: Example of an automated, high-throughput plant phenotyping system using linear actuators and a moving camera <sup>24</sup> .....	16
Figure 5: Photo of finished device in operation inside a MLR-352-PE growth chamber (Panasonic).....	22
Figure 6: Sequence of operations and decisions occurring within the main Python script. Ensures detection of indexing faults by calling index calibration protocol during error.....	22
Figure 7: Sequence of operations and decisions occurring within the index calibration protocol .....	23
Figure 8: Y-axis = colour hue. The hue in HSV colour space can range from 0-179, the lower the hue the more pink the average pixel value. X axis = sample number. Every sample represents the colour observed for a given image capture, over a total timespan of 12 days. ....	26
Figure 9: Y-axis = colour hue. The hue in HSV colour space can range from 0-179, the lower the hue the more pink the average pixel value. X axis = sample number. Every sample represents the colour observed for a given image capture, over a total timespan of 12-night cycles.....	26
Figure 10: Defining the minimum change required to classify a transition between white and pink colour.....	28
Figure 11: Growth of nematode without coloration change over two weeks.....	28
Figure 12: Root pinkness comparison between RUBY-8-3 (left) and RUBY-10-1 (right) .....	31

# List of Abbreviations

CN	Cyst Nematodes
CSV	Comma Separated Values
HSV	Hue Saturation Value
ISC	Initial Syncytial Cell
J1	Juvenile Stage 1
J2	Juvenile Stage 2
LEDs	Light Emitting Diodes
NPN	Negative Positive Negative
PAT	Portable Appliance Testing
PCB	Printed Circuit Board
PLA	Tough Polylactic Acid
PNG	Portable Network Graphics
PPNs	Plant Parasitic Nematodes
RGB	Red Green Blue
RN	Root Knot Nematodes
RPi	Raspberry Pi

# Chapter 1 - Introduction

## Plant parasitic nematodes (PPNs)

Nematodes (worm-like organisms), belonging to the phylum Nematoda, are the most abundant animals on our planet<sup>1</sup>. Their lifestyles are adapted to most ecosystems<sup>2</sup>, and may be either free-living (not requiring a host) or parasitic (dependant on a host). Plant parasitic nematodes (PPNs) have a grave impact on humans due to their impact on global crop yields, which threatens global food security and economic stability.

The plight of PPNs on global food security is illustrated by the fact that they can parasitise every major crop<sup>3</sup>, resulting in the destruction of 8.8-14.6% of global agricultural produce<sup>4</sup> (this excludes countries unable to carry out nematological studies). In terms of economic impact this translates to a worldwide loss of \$157 billion<sup>5</sup>; this loss is disproportionately borne by countries where agricultural production makes up a larger proportion of the gross domestic product. Cyst nematodes (CN) and root knot nematodes (RN) are the most damaging species<sup>6</sup>.

## Control measures

Many control measures exist to alleviate the impact of PPNs. Nematicides successfully eliminate the parasites but are often banned due to concerns over their impact on human health<sup>7</sup>, or offer poor control if approved for use<sup>8</sup>. Resistant cultivars are crops which possess a defence response conferred by resistant genes<sup>9</sup>. This control measure has seen widespread success in potato cultivation to resist infection of *Globodera rostochiensis*<sup>10</sup>, activating cell division and tissue regeneration processes in response to wounding stress<sup>11</sup>. Dormant nematodes are resilient to environmental conditions but become vulnerable to starvation outside a suitable host upon hatching. Trap crops can reduce the amount of dormant nematode cysts in the soil by inducing hatching without providing an appropriate host<sup>12</sup>, which stops nematodes completing their life cycle. However, *Solanum sisymbriifolium*, a successful trap crop, is also an invasive weed<sup>13</sup> which farmers are reluctant to introduce due to the difficult removal methods<sup>14</sup>. Below a certain population size, nematode populations can exist in the soil without causing major crop failure. Resistant or non-host crops can be introduced via calculated crop rotations to keep the nematode population below this threshold. However, unproductive fields may not be an economically viable option for a farmer<sup>15</sup>. No perfect control measures exist, as these

must balance factors such as effectiveness, cost, regulatory compliance, and development time. A combination of approaches is likely the best way to control nematode damage, therefore exploring new routes for control that can enrich a combination approach is worth investigating.

### Lifecycle of *Heterodera schachtii*

There are many modes of plant parasitism<sup>16</sup>: ectoparasites feed from outside the plant root, while semi-endoparasites only partly enter the host root. Migratory endoparasites spend most of their life cycle within the host, targeting different tissues. Lastly, sedentary endoparasites feed on one specific host feeding site. CNs are sedentary endoparasites and include economically relevant genera such as *Heterodera* and *Globodera*. This work concerns itself with investigating the behaviour of beet cyst nematode *Heterodera schachtii* by infecting *Arabidopsis thaliana* as a host plant.

An assay composed of *H. schachtii* and *A. thaliana* is the model system chosen to study nematode parasitism. This is due to the extensive research documenting their life cycle and genome, as well as the ease of culturing and maintaining them in laboratory setting, allowing for controlled and reproducible experiments. Furthermore, *A. thaliana* has abundant genetic tools available (mutant libraries) to facilitate genetic studies of plant defence against parasitism, and its transcriptional response to *H. schachtii* infection has been mapped.

The end of a female cyst nematodes life is denoted by tanning of the cuticle. Inside the body of the deceased female lie, sometimes up to a few hundred, eggs containing second stage infective juvenile nematodes (J2). In this state, nematodes may survive lying dormant for decades<sup>6</sup>. Once a suitable host is near, however, hatching from the egg is induced via recognition of host specific signal molecules<sup>17</sup>. Through mechanical thrusting using a needle like stylet located in the head part to break open the egg, the nematodes are released, and enters a window of survival during which it must find a host before exhausting its resources.

Once the J2 has found the host, it penetrates the root epidermal cells using its stylet and migrates to the vascular cylinder. Here it uses its stylet to probe for an appropriate cell to establish a feeding site. This is done by inserting the stylet into the cell and injecting effectors to initialise the formation of the initial syncytial cell (ISC)<sup>18</sup>. Effectors are proteins injected into the plant that manipulate its biology to enable infection by

the parasite<sup>19</sup>. After a period of preparation, the nematode begins to extract nutrients from the ISC via a feeding tube. The ISC and adjacent cells undergo structural changes, degradation of cell walls and fusion of plasma membranes incorporate them into a single multinucleate hyper metabolically active feeding organ, termed the syncytium.

Thus far, the nematode remains sexually undifferentiated. The precise mechanism for sexual differentiation is unknown but is widely believed to be determined by nutrient availability at the syncytium<sup>20</sup>. To reach sexual maturity, both males and females go through various moulting stages. Female nematodes remain attached to the syncytium for the rest of their life cycle, whereas males regain their vermiform shape and migrate to mate with females. Inside mated females, eggs, each containing an embryo develop into a first-stage juvenile (J1), which later molts into J2. Eventually, mated females tan (harden), die, and turn into cysts which protect the dormant J2s for up to a few decades, until favourable conditions stimulate hatching.

## **Observation and hypothesis**

A fundamental tenet in parasitology is that a more complete understanding of host-pathogen interactions enables development of novel or more effective means of control.

### **Preliminary observation**

Typically, nematode phenotyping is performed under the microscope, resulting in the observation of a static timepoint of parasitism. In recent years, the lab has worked on the development of machinery and computer vision approaches to largely automate the above-mentioned assay (unpublished). The system most notably enables studying parasitism through time.

Saswata Dey, (PhD student Department of Plant Sciences), who has developed betalain expressing *A. thaliana* lines (e.g.: RUBY-8-3), giving them a pink or purple appearance, noticed that nematodes can take up this substance, and break it down over time, in cycles (Figure 1). At any given time, some nematodes are pink, and some are not, and over time some nematodes appear to alternate between pink and white repeatedly.

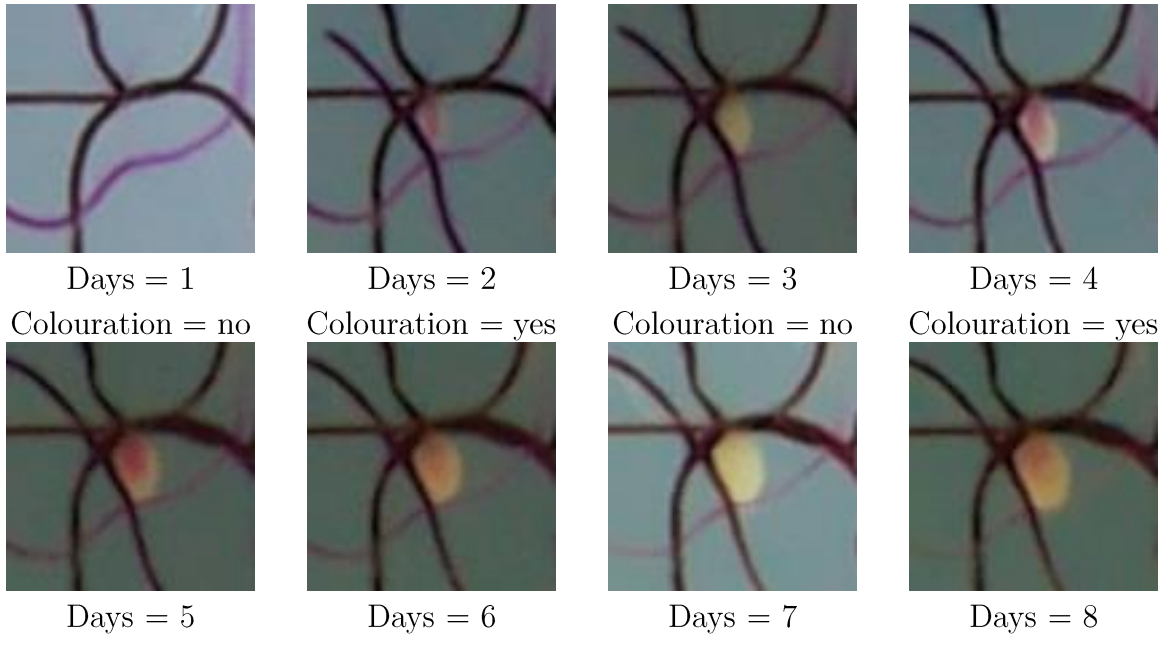


Figure 1: From left to right, top then bottom, the growth and variation in pink colour of a nematode over 8 days.

We hypothesise that the acquisition of pink colour is an indicator of nematode nutrient uptake from the roots, and that the loss of pink coloration is an indicator for digestion of nutrients. However, the frequency of imaging in the output of the current machinery is not sufficient to develop a model of nematode feeding behaviour. Figure 2 demonstrates how the coloration values from Figure 1 can lead to over or underfitting, highlighting the need for higher time resolution.

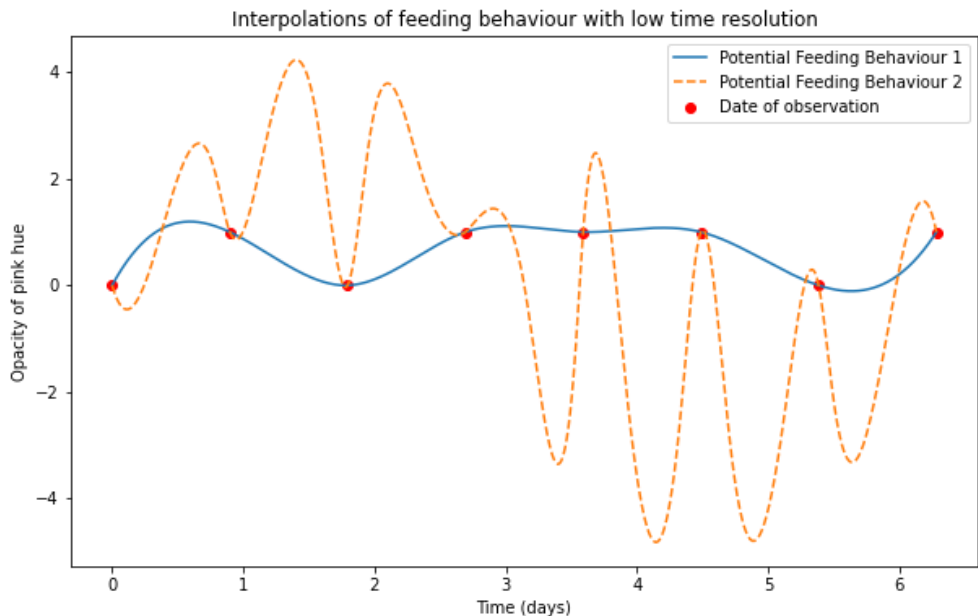


Figure 2: Over and underfitting of data with low time-resolution. Y-axis = presence of pink. X-axis = sample number. Every sample represents the colour observed for a given image capture, over a timespan of 8 days.

### **Hypothesis and investigative rationale**

If pinkness can serve as an indicator of feeding, graphs tracking the fluctuating values of pinkness (and therefore feeding) may be generated by imaging with a higher time resolution, elucidating features such as the frequency, regularity, and intensity of nematode feeding. Understanding nematode feeding behaviour may help develop more effective control measures against nematode plant parasitism, by discovering if feeding is a cyclic behaviour, how long feeding cycles are, and whether or not they can be disrupted.

# Chapter 2 - Literature review

## Feeding behaviour

Most of the literature investigating the feeding behaviour of *Heterodera schachtii* was published before the year 2000, using *in vivo* assays combined with contrast microscopy techniques. At first, observation and dissection demonstrated the fundamental feeding pattern, wherein nematodes protrude their stylet into a modified plant cell, release secretions, and subsequently ingest nutrients through the pulsation of the median bulb<sup>21</sup>.

Then, research by Wyss and Zunk<sup>22</sup> corroborated these findings, specifically for *H. schachtii* within the roots of *Brassica napus*. Detailed analyses were facilitated by video-enhanced contrast microscopy, enabling close observation of the feeding process within the root tissues of model host. Three distinct phases were identified in the feeding cycle, which are repeated throughout development and interrupted only during moulting. Phase I involves continuous withdrawal of nutrients from the syncytium through a feeding tube. In phase II, the stylet is retracted and re-inserted as secretory fluids are depleted. Phase III is characterized by the movement of new secretory fluids into the syncytium. This cyclic pattern persists throughout the development of both males and females.

Wyss and Grundler<sup>23</sup> delved further into the observation of the initial syncytial cell formation and feeding cycles, replacing the host with *Arabidopsis thaliana* which has translucent roots and greater utility for imaging via video-enhanced contrast microscopy. At J2 stage, *H. schachtii* possess a large robust stylet, enabling them to penetrate root tissues by overcoming cell wall barriers through mechanical force. After selecting a viable cell within the vascular cylinder to be transformed into the ISC, J2s undergo an extended quiescent period characterized by minimal feeding activity, during which they transition from a migratory to a sedentary form. The lack of defecations observed during this period suggests that secretions from the subventral oesophageal glands are passed into the intestine, potentially aiding in the mobilization of lipid reserves, and preparing the intestine for subsequent nutrient absorption. The dorsal gland secretions in sedentary *H. schachtii* serve at least three functions: stimulating syncytium formation, modifying the cytoplasm at the feeding site, and providing feeding tubes for nutrient withdrawal. These feeding tubes are likely formed through the interaction of dorsal gland secretions with the cytoplasm and are necessary for efficient nutrient uptake.

*Heterodera schachtii* exhibit three distinct feeding phases that are repeated cyclically throughout development, indicating a need to periodically renew the conditions for efficient nutrient withdrawal from the syncytium. Wyss and Grundler investigated 68 feeding cycles for one individual J2, from the beginning of feeding until moulting, quantifying the durations of the different phases. Phase III lasted on average 25 minutes, Phase II lasted on average 5 minutes, and Phase I had more variable durations, increasing from 30 to 60 minutes as the nematode neared moulting.

## Imaging limitations

Video-enhanced contrast microscopy provided a great capacity for precise observation of nematode feeding. Unfortunately, Wyss and Grundler do not contextualise their observation by detailing the regularity with which nematodes are feeding; that is, the elapsed time between any three feeding phases. It is not clear if the imaging was automated, and therefore continuous, or if interruptions in recording existed. A figure they produced (see Figure 3) suggests 67h and 15min elapse from first feeding to moulting, which is not representative of typical nematode lifespan. The quantitative observation of phase durations is only available for one nematode rather than the whole population infecting the plant. These instances of missing experimental details are perhaps due to the constraints of the imaging technology available during the study. Despite the valuable insights into feeding phases, Wyss and Grundler fail to elucidate the frequency and continuity of *H. schachtii* feeding over an individual nematode's lifetime, as well as possible consequence on growth and moulting.

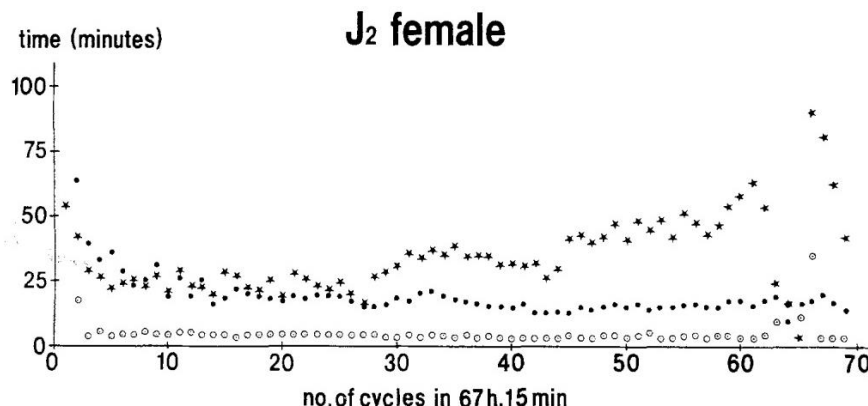


Fig. 2. Number of feeding cycles in a selected *Heterodera schachtii* juvenile stage 2 (J2) female nematode from beginning of feeding until last stylet retraction before beginning of moult, and duration of feeding phases. , = phase I (continuous food infestation); followed by phase II (time between stylet retraction and reinsertion into feeding site), represented by white spots; followed by phase III (forward flow of secretory granules through extensions of oesophageal glands, especially dorsal gland), represented by black spots; followed again by phase I.

Figure 3: Duration of feeding phases of female *H. schachtii* adapted from Wyss and Grundler<sup>23</sup>

An important improvement to the imaging capability of Wyss and Grundler is the ability to record data continuously and autonomously via automation, to operate when researchers are not present. Furthermore, digitisation of experiments (photographic data) enables long-term storage, allowing for analysis post experimentation, as well as leveraging of computational tools for analysis. In addition, capturing all the nematodes on the host generates many more data points. Due to the semi-random nature of gene expression and biological processes, a large volume of observations is required to draw statistically significant conclusions. Various examples of these technological features exist, especially in the field of plant phenotyping. The design of hardware, required to generate data, and computational analysis tools, to extract information from the data, are essential and distinct components of the imaging method. For example, Lee et. Al.<sup>24</sup> developed an automated, high-throughput plant phenotyping system that can reliably acquire and analyse large-scale plant image datasets. The hardware, seen in Figure 4, allows for automated image acquisition of many plant samples while minimizing plant stress, utilising a system of linear actuators to move a camera in 3D space. The software component consists of a machine learning-based automated pipeline for plant image segmentation and analysis.

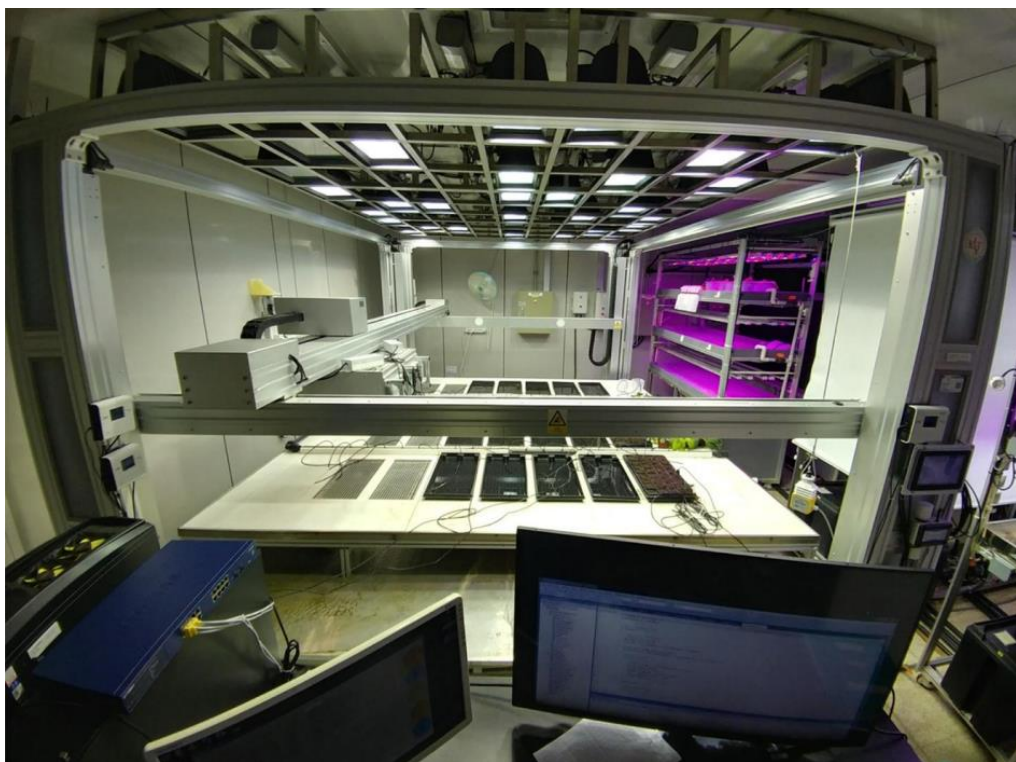


Figure 4: Example of an automated, high-throughput plant phenotyping system using linear actuators and a moving camera<sup>24</sup>

# Chapter 3 - Materials and methods

## Biological methods

### Axenic culture of *Heterodera schachtii* on *Arabidopsis thaliana*

*Arabidopsis thaliana* seeds (RUBY-10-1) with a betalain expressing gene were obtained internally, surface sterilised with 20% v/v bleach (ThermoFisher) for 20 minutes and washed six times with sterile double-distilled H<sub>2</sub>O. To improve and synchronise germination, the seeds were kept at 4°C overnight <sup>25</sup>. They were then sown on 50 mm petri dishes (Sarstedt) containing a water and agar solution. The plants' growth cycles consisted of a 16-hour day at 21°C and an 8-hour night at 20°C in the MLR-352-PE growth chamber (Panasonic).

Cysts were soaked in 3 mM Zinc Chloride solution (Sigma-Aldrich) to promote hatching<sup>26</sup> in a specialised hatching jar (Jane Maddern Cosmetic, 250mL) with two 2.5 cm plastic rings (alt-intech Tube Perspex) holding a 20 µm mesh (Sigma-Aldrich). Five days after hatching, the J2 nematodes that passed through the mesh were collected with a pipette. They were washed five times with a sterile double-distilled H<sub>2</sub>O with 0.01% v/v Tween (Sigma-Aldrich), termed "nemawash". The density of nematodes was adjusted to 1 nematode/µL using sterile nemawash. At four weeks post germination, roots of *A. thaliana* were inoculated with 80 J2 nematodes by pipetting the suspension onto the roots.

## Engineering methods

### Introduction to engineering methods

Design requirements were laid out to permit retrospective assessment of device performance once built. These aim to ensure high quality data is produced (image quality and throughput, and consistent dish indexing), that the device does not invalidate the existing biological methods (compatibility with biological methods), and that the device functionality needs are met by using appropriate components (electronic components). In Table 1, the high-level design requirements of the device are displayed.

## Design requirements

Table 1: Device design requirements (numbered requirement IDs)

Purpose	Design requirement
1. Image quality	<ol style="list-style-type: none"> <li>1. The full circumference of the dish shall be visible on captured images.</li> <li>2. The camera shall capture 12MP images.</li> <li>3. The images shall be saved without any loss of quality.</li> <li>4. The camera shall be focused to the dish distance.</li> <li>5. Even lighting shall turn on around the dish during image capture.</li> <li>6. The device shall isolate the dish from external light sources during imaging.</li> </ol>
2. Image throughput	<ol style="list-style-type: none"> <li>1. The device shall photograph each dish a minimum rate of 1 image per hour.</li> <li>2. The device shall be capable of imaging 14 dishes contemporaneously.</li> <li>3. The device shall have storage capacity for a minimum of 100,000 images.</li> </ol>
3. Compatibility with biological methods	<ol style="list-style-type: none"> <li>1. Lighting shall minimise impact on the plant lifecycle.</li> <li>2. Lighting shall only turn on during image capture or index calibration.</li> <li>3. Lighting shall turn on for only one dish at a time.</li> <li>4. The device shall fit inside the Panasonic MLR-352-PE growth chamber (max base width 470x500 mm).</li> <li>5. The device surfaces shall be compatible with cleaning products such as isopropyl alcohol.</li> <li>6. The device shall be compatible with a Sarstedt 150 mm sterile petri dish.</li> </ol>
4. Indexing	<ol style="list-style-type: none"> <li>1. The device shall assign a unique index to each dish.</li> <li>2. The device shall have a means of verifying the index of an imaged dish.</li> <li>3. The device shall have a means of recalibrating dish indexes in case of indexing failure.</li> </ol>
5. Electronic components	<ol style="list-style-type: none"> <li>1. The device shall have a means of moving dishes into the appropriate position for imaging.</li> <li>2. The device shall have a means of detecting when a dish reaches the appropriate position for imaging.</li> <li>3. The device shall have a means of holding the dishes in the appropriate position during imaging.</li> </ol>

	<p>4. The device shall have a means of supplying 5V, 12V, and 24V.</p>
	<p>5. The device shall have means of wiring controllers, sensors and actuators.</p>
	<p>6. The device shall have a means of displaying operational status, sample photos, and receiving commands from a user.</p>

## Hardware design rationale and implementation

The central controller of the device was the Raspberry Pi (RPi) 4B 8GB RAM (RASPERRY-PI). A custom circular carousel was designed to hold the Sarstedt dishes, which spins about its centre on two flange bearings (RS PRO) (see ‘Appendix - Engineering methods’ for detailed drawings and a bill of materials).

### Image quality

The image quality requirements were defined to minimise the loss of information in the produced image dataset, allowing for richer extraction of quantitative features in later computer-vision analysis. To this end, the 12 MP RPi-HQ-Camera (RASPERRY-PI) interfaced with 16 mm Telephoto Lens (RASPERRY-PI) was used. An imaging chamber was designed to exclude external light sources, inside which the camera faced (up toward) the bottom of the imaged dish, and both elements were housed in an opaque enclosure. A focal distance of 150 mm between the camera lens and the bottom of the imaged dish was implemented to keep the dish in frame and in focus. The imaged dish was surrounded with a 12V Green LED Strip Light (Inexstation). The images were saved in portable network graphics (PNG) format which benefits from lossless compression.

### Image throughput

The image throughput requirements were defined to ensure the produced dataset is large enough that statistically significant observations can be made. Typically, a number of samples  $n = 30$  is desired, but due to space limitations  $n$  was reduced to 14 dishes. The device was designed to have an average imaging rate of 4 photos per dish per hour. The spinning carousel was designed to permanently carry 14 dishes. A 2 TB hard drive (Seagate) was interfaced with the RPi to store the images.

## Compatibility with biological methods

These requirements were designed to ensure seamless compatibility between the device and existing biological methods. Green light emitting diodes (LEDs) were chosen to minimise the impact of sudden light exposure on plants' endogenous timing mechanisms<sup>27</sup>. Each dish was surrounded by LEDs, which were only turned on when the dish in question was imaged, to minimise frequency and duration of sudden light exposure. The LEDs were controlled through a negative positive negative (NPN) transistor circuit, controlled via an Arduino Uno (Arduino) interfaced with the RPi using the I2C protocol (see 'Appendix - Engineering methods' for I2C detail). A custom PCB was designed to fit 14 independent switching circuits (see 'Appendix - Engineering methods' for circuit diagrams and PCB design). To ensure compatibility with the growth chamber, a polycarbonate baseplate was used for its robustness, cut to 450x490 mm, upon which all device components were mounted. Materials used in the build included acrylic, polycarbonate, and tough polylactic acid (PLA) (ULTIMAKER) to allow wiping down with cleaning products.

## Indexing

Indexing requirements were designed to ensure that photos of different dishes in the dataset can easily be sorted into groups. They also ensure that the dish being photographed is saved with the correct index and received the appropriate lighting. An indexing protocol was designed to fulfil these requirements. To find out which dish was currently in the imaging chamber, all LEDs were turned on sequentially, and a photo was taken each time. Each time a photo was taken, the number of the switched LED pin was assigned to the photo. Then, the light intensity for each photo was calculated by the RPi using the average pixel value of three colour channels, producing an indexed set of light intensity values (see 'Appendix - Engineering methods' for main Python script). Whichever value in this set is highest is the index of the dish currently in the imaging chamber. Photos were saved with a title containing the index, followed by a timestamp, ensuring chronological storage and straightforward sorting. During normal operation, a light intensity threshold verified photos taken had LEDs on and therefore that the indexing was accurate. If this was not the case due to device failure, the indexing protocol begins again. QR codes labelled 1-14 were printed on an adhesive and stuck to the bottom of the dishes to recuperate index numbers in case of index failure.

## Electronic components

The electronic design requirements ensure the device possesses adequate components for actuation and detection of dish movement, appropriate power supply and wiring, and an interface with the user. The spinning carousel which contains the dishes was driven by the 12V worm geared DC motor (YOSOO). The motor was tensioned into contact with the outside diameter of the carousel with a spring. A band of rubber was glued around the motor's rigid shaft coupling (CNC Planet) to ensure grip between the motor and the outer diameter of the carousel. The carousel also contained a slot for neodymium magnets (YIZHET) adjacent to every dish, on the outer edge of the carousel's diameter. On the edge of the imaging chamber was a hall effect sensor (Waveshare) to determine when a dish has passed into the imaging chamber. Hall effect sensor placement was such that when dish of index  $n-1$  is detected, the motor is stopped, placing dish of index  $n$  in the imaging chamber. On the other side of the imaging chamber, the 24V 280N access control door magnet (RS PRO) was turned on to attract the magnet adjacent to dish of index  $n+1$ . This ensured central positioning of dish of index  $n$  inside the imaging chamber regardless of motor spin-down time. A custom power supply was designed by combining the triple output 136W switching power supply (MEAN WELL), the C14 panel mount IEC male connector (Bulgin), then fixed in an enclosure and portable appliance testing (PAT) tested. A 6-wire slipring (PI HUT) was used to connect the Arduino on the spinning carousel with the RPi on the baseplate, allowing the wires to spin freely. Other connections were made using the JST HX connector kit (WOSHILAO LABS). Finally, the 7-inch touchscreen display (PI HUT) was connected to the RPi to allow the user to read device operation progress, inspect existing images, and start/stop the imaging sequence.

## Fabrication methods

The carousel was laser-cut out of transparent acrylic. The polycarbonate baseplate was cut using a bandsaw. All enclosures and component mounts were designed in Fusion 360 (Autodesk) and 3D printed using the S3 3D Printer (UltiMaker). The LED switching PCB was designed using DipTrace and produced using etching, drilling, and via pressing. The finished device can be seen in Figure 5.

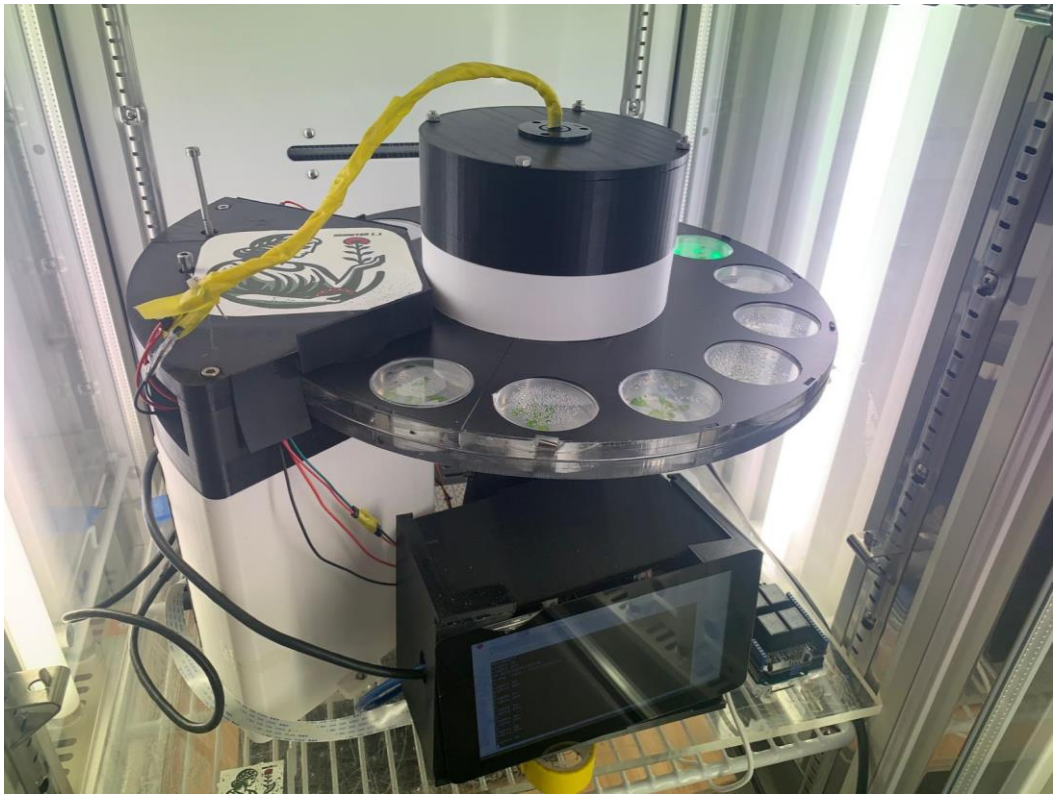


Figure 5: Photo of finished device in operation inside an MLR-352-PE growth chamber (Panasonic).

## Logic flow diagrams

The logic flow diagram in Figure 6 represents the sequence of operations, decisions, and processes within the device upon initialisation of the main Python script. This assumes successful powering up and boot sequence of the RPi (see ‘Appendix - Engineering methods’ for main Python script).

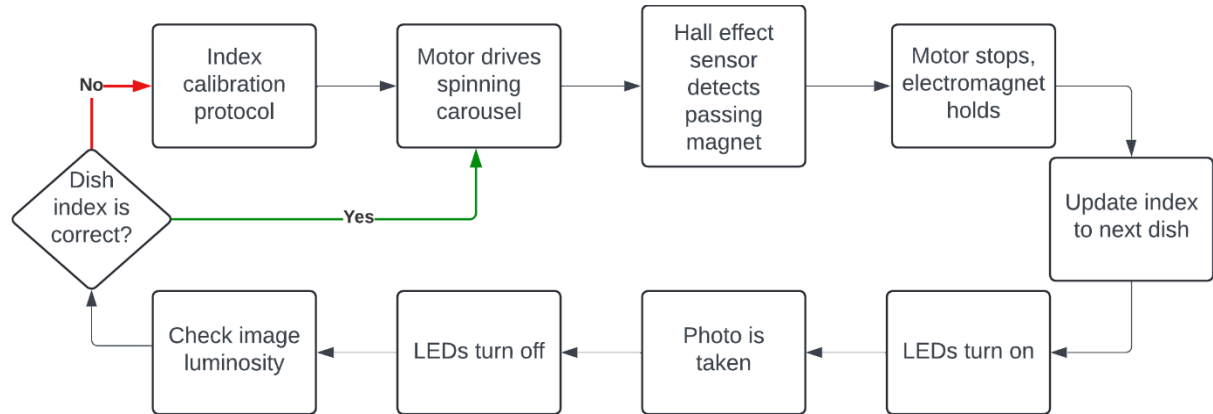


Figure 6: Sequence of operations and decisions occurring within the main Python script. Ensures detection of indexing faults by calling index calibration protocol during error.

The logic flow diagram in Figure 7 displays the index calibration protocol allowing the device to correctly assign an index value to the dish in the imaging chamber.

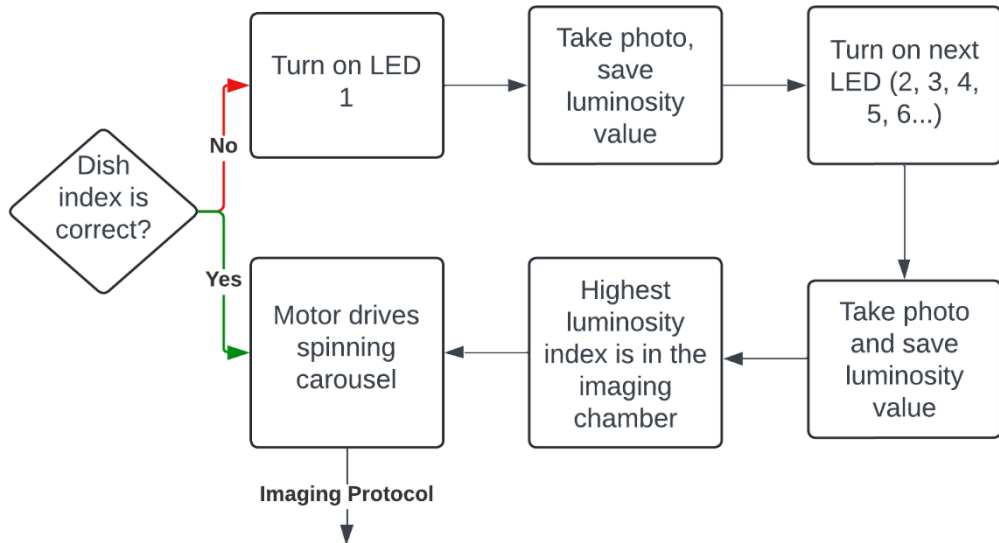


Figure 7: Sequence of operations and decisions occurring within the index calibration protocol.

### Image processing pipeline

A semi-automated image processing pipeline was designed to extract information from the images generated by the device. First, the images were grouped according to the dish index. Then, the ImageJ virtual stack function was used to align all images of a given dish, ensuring that the pixel coordinates for any nematode would be constant throughout the dataset. Then, manual segmentation of the inside of the nematodes was carried out in ImageJ, producing a list of ‘coordinate boxes’ exported as a comma separate value (CSV) file. Finally, the CSV file containing the nematode coordinates, and the aligned dataset, were passed to a Python script.

The Python script first segmented the nematode on every image by using the manually provided coordinates. Each dish therefore contained sub-datasets equal to the number of nematodes present on the root network. The average hue saturation value (HSV) (colour-space measurement alternative to RGB, intended to describe hue in a human-intuitive way) value was calculated for each nematode and recorded through time. Finally, a dataset of mean HSV value over time for each nematode on each dish was obtained, ready for analysis (see ‘Appendix - Engineering methods’ for image processing Python script).

# Chapter 4 - Results

## Device performance

In Table 2, the performance of the device is evaluated by assessment against the design requirements laid out in Table 1. Out of 24 design requirements, 4 were not satisfactorily met, and the cause for failure is outlined in the table. The other requirements were successfully met.

Table 2: device performance evaluation against design requirements.

Purpose	Design requirement
1. Image quality	<ol style="list-style-type: none"><li>1. FAIL – the full circumference of the dish is not visible, focal distance too small.</li><li>2. PASS – 12MP images.</li><li>3. PASS – PNG lossless compression.</li><li>4. PASS – camera focus accessible and tuneable.</li><li>5. FAIL – LED quality and diffusion inappropriate for even lighting.</li><li>6. FAIL – transparent carousel and gaps at entrance of imaging chamber allowed excess ambient light through</li></ol>
2. Image throughput	<ol style="list-style-type: none"><li>1. PASS – imaging occurs at minimum rate of 1/hour.</li><li>2. PASS – 14 dishes fit on the carousel.</li><li>3. PASS – 2TB storage sufficient for 600,000 images.</li></ol>
3. Compatibility with biological methods	<ol style="list-style-type: none"><li>1. PASS – green lighting used.</li><li>2. PASS – LEDs not powered unless imaging or calibrating.</li><li>3. PASS – Arduino I2C protocol controls 1 LED at a time.</li><li>4. PASS – device baseplate area = 450x490 mm.</li><li>5. PASS – device surfaces made of polycarbonate, acrylic and tough PLA, electronics are enclosed.</li><li>6. PASS – carousel holes equal to dish dimension + 2mm tolerance.</li></ol>
4. Indexing	<ol style="list-style-type: none"><li>1. PASS – each dish indexed between 1-14.</li><li>2. PASS – index validation via luminosity measurement.</li><li>3. PASS – successful index calibration protocol.</li></ol>
5. Electronic components	<ol style="list-style-type: none"><li>1. PASS – worm geared motor, spring tensioner, and rubber coated shaft coupling.</li><li>2. PASS – neodymium magnets and hall effect sensor.</li><li>3. FAIL – electromagnet and neodymium magnet distance too large to exert appropriate holding force.</li></ol>

	<p>4. FAIL – 5V 2A switching power supply cannot provide sufficient RPi power due to numerous peripherals.</p>
	<p>5. PASS – slipring connection for spinning components and JST connectors for other components.</p>
	<p>6. PASS – touchscreen display allows user input and display of operation and images.</p>

### Mechanism for tracking colour change

The core working principle of the device and the dataset of images produced is the ability to detect the increasingly pink hue of nematodes as they ingest betalain in the feeding site, as well as detecting the loss of the pink hue upon nematode digestion. The mechanism for detecting gained pink colouration is shown to work in Figure 8. The mechanism for detecting lost pink colouration is shown to work in Figure 9.

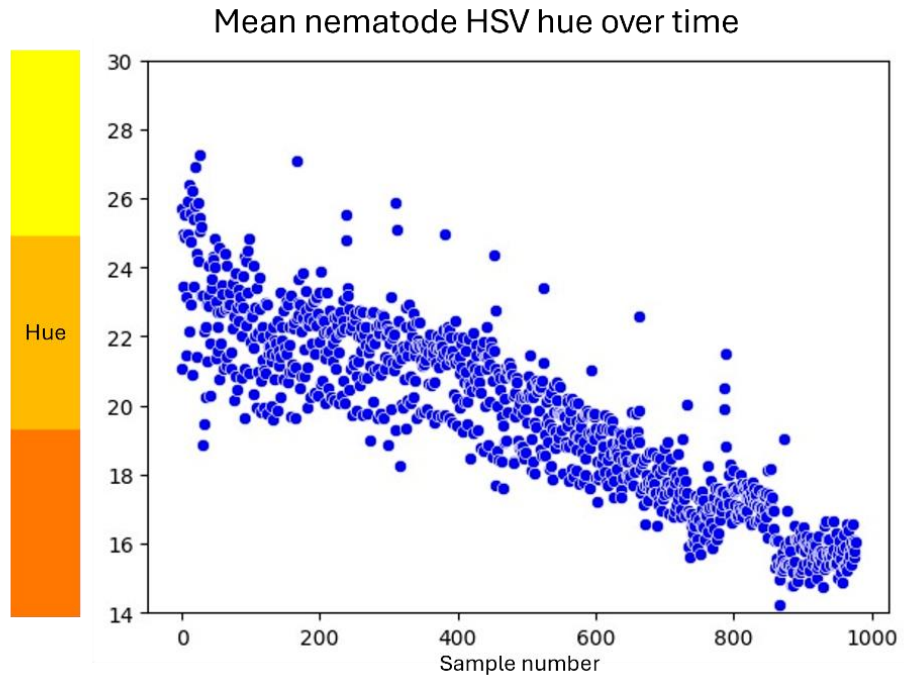


Figure 8: Y-axis = colour hue. The hue in HSV colour space can range from 0-179, the lower the hue the more pink the average pixel value. X axis = sample number. Every sample represents the colour observed for a given image capture, over a total timespan of 12 days.

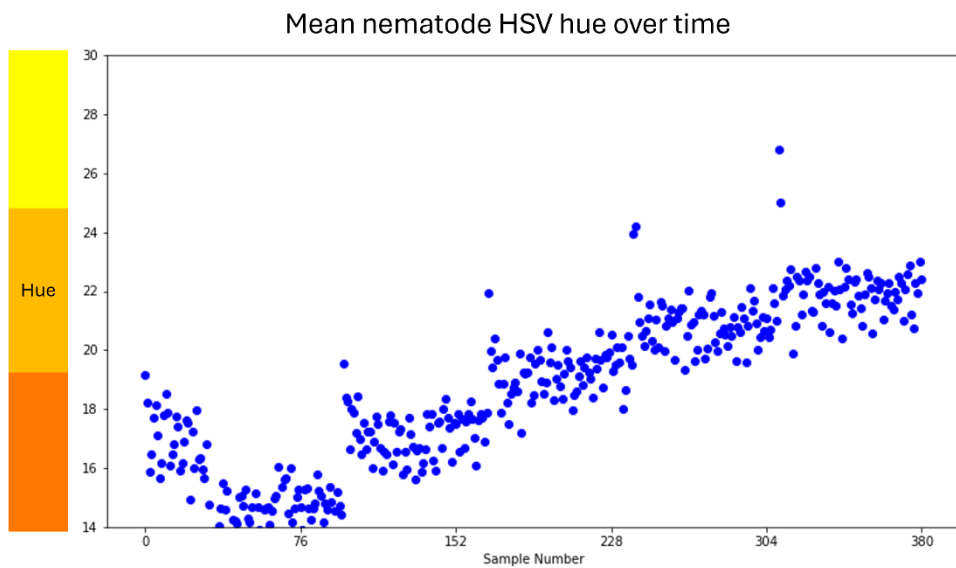


Figure 9: Y-axis = colour hue. The hue in HSV colour space can range from 0-179, the lower the hue the more pink the average pixel value. X axis = sample number. Every sample represents the colour observed for a given image capture, over a total timespan of 12-night cycles.

Unsuccessful attempts were made at detecting colour change in the RGB colour space, see 'Appendix – data analysis' for detail.

## Observed feeding behaviour

The observed colour-change of nematode populations in all 14 dishes, displayed in Table 3, demonstrates that only a minority of nematodes changed between white and pink (14%). The remainder of the nematodes either acquired pink from the beginning of their feeding (41%) and never lose it, or never acquired any pink (45%). Examples of the minimum imaged colour difference required to classify a nematode as changing between pink and white are given in Figure 10.

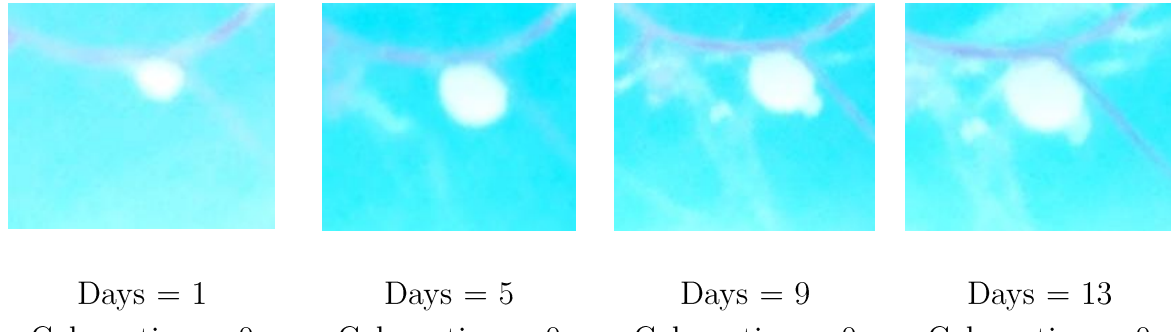
*Table 3: Observed nematode colouration over all imaged individuals. Total individuals = 293, individuals changing colour = 43.*

Plate number	Nematode remains white	Nematode remains pink	Nematode changes between white and pink
1	26	0	0
2	3	21	0
3	7	15	3
4	5	11	2
5	7	12	3
6	4	13	2
7	7	18	4
8	19	0	1
9	5	4	4
10	8	2	4
11	15	5	8
12	2	10	7
13	19	1	2
14	4	7	3
<b>SUM</b>	<b>131</b>	<b>119</b>	<b>43</b>



*Figure 10: Defining the minimum change required to classify a transition between white and pink colour.*

Furthermore, Figure 11 shows that for a selected nematode identified as remaining white, growth can be distinctly observed as the size of the nematode increases over time.



*Figure 11: Growth of nematode without coloration change over two weeks.*

# Chapter 5 - Discussion

## Device performance evaluation

### Proposed design modifications

Table 4 below outlines why the device fails to meet some of the initial design criteria and proposes modifications to overcome these problems. Despite these unmet criteria, the device was able to produce a dataset of over 50,000 images over the course of 3 weeks.

*Table 4: Proposed solutions for failed design requirements (see Table 1 for requirement ID).*

Requirement ID	Proposed solution
1.1	Full dishes are out of frame. The carousel mount and imaging chamber should be raised by 30 mm by 3D printed spacers matching their bottom surface shapes. The camera mount should not be raised by these spacers, increasing the distance between the lens and the bottom of the dish to 180 mm.
1.5	The Inexstation LED strips were inadequate as they lacked a light diffuser and did not have high quality control of light wavelength, resulting in colour variation across some images. These should be replaced with high quality green LEDs coated with a light diffuser.
1.6	The transparent carousel and openings either side of the imaging chamber failed to isolate external light. The existing carousel should be spray painted black, or a new carousel should be laser cut out of black acrylic. Flexible rubber sheets should be glued to the edges of the imaging chamber to seal the surface while conforming to the forces of the spinning carousel.
5.3	The carousel magnets were out of range of the magnetic field exerted by the electromagnet, due to the high distance between the components. An alternative mechanism for restraining a spinning part should be used. A ball plunger would engage with semicircular divets on the surface of the carousel as the motor spins down. Upon powering of the motor, the resistance of the ball plunger would be overcome, and it would leave the divet, allowing the carousel to spin freely until the next dish is reached.
5.4	The RPi suffered from low power issues and was powered using the original power supply adapter. This was due to excess power demand caused by numerous peripherals interfaced with the RPi. The custom power supply voltage can be scaled through a potentiometer on the

	linear regulator. Therefore, the power requirements of the RPi should be tested with all peripherals active, and the output voltage of the 5V channel scaled accordingly.
--	---

Furthermore, assessing device performance elicited additional modifications to increase the rate of imaging. Firstly, occasional slipping occurred between the rubber coated motor shaft coupling and the outer edge of the acrylic carousel. This led to variability in the rate of imaging. To prevent the issue in future, the outer edge of the carousel should also be coated with rubber, or adhesive-backed sandpaper.

The hall effect sensor occasionally failed to detect a passing magnet, triggering the indexing calibration protocol, reducing the rate of imaging. This system is prone to variability due to magnets having varying strengths, and an exponential reduction in strength with increased distance from sensor to the edge of the carousel. A more robust solution consists in replacing the magnets with upward or downward plastic protrusions and replacing the hall effect sensor with a photoelectric sensor. This sensor would trigger every time a protrusion passed through its gates, irrespective of protrusion composition and age, and unaffected by small distance variations, unlike in the case of magnets.

### Device applicability

It is apparent from Table 3 that the fluctuating pattern of nematode pink colour expected following Saswata Dey's experiment have not obtained. In cases where colouration is not an available indicator of the feeding behaviour of the nematodes, the device remains valuable research tool in answering novel questions by virtue of its unique high time-resolution imaging capabilities. The images produced contain multiple features that can be extracted, such as nematode size, shape, location on the roots, distance between individuals and colour changes over nematode lifecycle. These higher time-resolution features may prove useful in investigating nematode behaviour further, as well as investigating the effectiveness of plant resistance genes.

The causes behind the difference from Saswata Dey's dataset could be numerous. The major differences the device introduced to the experimental setup are regular spinning of hosts and parasites and frequent sudden green light exposure.

## Experimental evaluation

### Experimental failures

As mentioned above, no cyclical feeding as in Saswata Dey's experiment was observed due to unforeseen circumstances. Graphs tracking the fluctuating pinkness of nematodes, as suggested in the hypothesis, were not obtained. Instead Figure 8 and Figure 9 demonstrated only that changing pinkness can be tracked. Therefore, the issue does not lie in the mechanism for tracking colour change, but in the experimental differences between the two experiments.

Firstly, different lines of *Arabidopsis thaliana* were used, RUBY-10-1 instead of RUBY-8-3. The latter, which led to the initial observations, has a lower epigenetic silencing probability of the betalain expressing genes. This may lead to a higher concentration of betalain in the nematode feeding sites, producing more effective colour changes in the nematodes. However, side by side comparison of RUBY-10-1 and RUBY-8-3 roots does not indicate an obvious difference in pinkness, as seen in Figure 12.

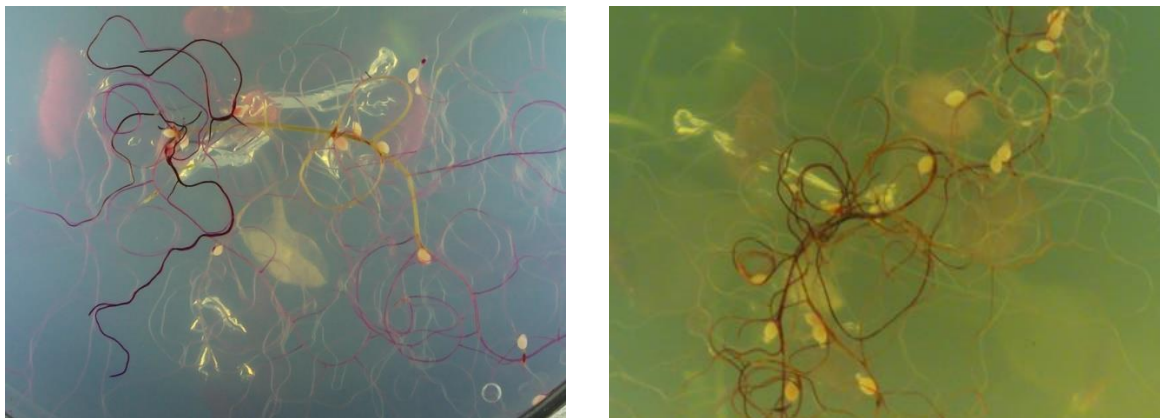


Figure 12: Root pinkness comparison between RUBY-8-3 (left) and RUBY-10-1 (right)

Green LEDs were chosen as they have much lower impact on plants' endogenous timing mechanisms than either blue or light<sup>27</sup>. However, this does not mean that green light has no impact on the plant, and the regular illumination occurring in the imaging chamber, throughout the plant's day and night cycles, may disrupt both the host and the parasite, leading to the observed change in feeding behaviour. Furthermore, placing the host-parasite system in a spinning carousel may also cause stress in the biological systems. Research surrounding positive and negative geotropism has shown that growth on a spinning disc leads to variability in the alignment of plant roots and shoots<sup>2829</sup>.

Imaging only began 12 days after nematodes inoculation, unlike Saswata Dey's experiment where it started 7 days after inoculation. Feeding behaviour may change in the later stages of a nematode's life cycle, which may also contribute to the differences in observed colour changes.

### **Disruption of feeding cycles**

Comparisons have been made between Saswata Dey's experiment, and the one carried out using the high time-resolution device. This is because the biological methods employed are identical, and variation is only introduced in the imaging methods. However, biological experiments are highly sensitive to variation, so the fragility of drawn comparisons should be noted. Nevertheless, the difference in observed colouration between these two experiments suggests that some component or process of the high time-resolution imaging device may be able to disrupt nematode feeding behaviour. This positive accidental discovery supports further investigation of how nematode feeding can be disrupted through sudden light exposure, experiencing unusual forces, or other variable experimental conditions. Translation of this theoretical control of behaviour into agriculture could ultimately produce a new method of nematode control.

### **Uncoloured nematodes**

There is a stark difference in the number of nematodes which never gain pink colour in Saswata Dey's experiment, and the one carried out using the device. As shown in Figure 11, the lack of pink colour does not prevent nematodes from growing, which suggests that feeding is occurring but not producing an increased pink colour. As it has already been mentioned, the variation in genetic line between the two experiments may explain this phenomenon. A less likely explanation is in the variation between nematodes, which might produce different levels of selectivity for betalain during feeding, or different metabolic rates upon feeding which cause faster digestion or changes to how ingested material is displayed on the nematode's exterior.

## Chapter 6 – Conclusion

This work has aimed to build on the existing imaging capabilities in the field of nematology by designing a device capable of automated high time-resolution imaging. The device was employed in the investigation of *Heterodera schachtii* feeding behaviour using betalain expressing *Arabidopsis thaliana* plants (RUBY-10-1). The design was made compatible with existing axenic culture methods. Most design specifications were met, leading to the production of a dataset containing over 50,000 images of nematodes over three weeks of observation. Proposed device modifications to meet all design requirements and improve the rate of imaging are also outlined. The hypothesised cyclical feeding behaviour of nematodes could not be observed, and several candidates are presented as potential causes for this. Nonetheless, it has been demonstrated that changing nematode pinkness can be quantitatively tracked over time, and that the device can produce large datasets of high time-resolution images.

# References

1. Van Den Hoogen, J. et al. Hiroaki Okada 37 , Juan emilio Palomares rius 38 , Kaiwen Pan 39 , Vlada Peneva 40 , loïc Pellissier 41,42 , Julio carlos Pereira da Silva 43 , camille Pitteloud 41 , thomas O. Powers 33 , Kirsten Powers 33. *Sara Sánchez Moreno* 22,
2. Drake, N. Subterranean worms from hell. *Nature* (2011) doi:10.1038/NEWS.2011.342.
3. Nicol, J. M. et al. Current Nematode Threats to World Agriculture. *Genomics and Molecular Genetics of Plant-Nematode Interactions* 21–43 (2011) doi:10.1007/978-94-007-0434-3\_2.
4. Singh, S. K., Hodda, M. & Ash, G. J. Plant-parasitic nematodes of potential phytosanitary importance, their main hosts and reported yield losses. *EPPO Bulletin* 43, 334–374 (2013).
5. Afzal, A. & Mukhtar, T. Revolutionizing nematode management to achieve global food security goals - An overview. *Heliyon* 10, (2024).
6. Jones, J. T. et al. Top 10 plant-parasitic nematodes in molecular plant pathology. (2013) doi:10.1111/mpp.12057.
7. Change required from top to bottom - Crop Production Magazine. <https://www.cpm-magazine.co.uk/roots/change-required-from-top-to-bottom/>.
8. Trial shows best nematicide strategy for PCN in potatoes - Farmers Weekly. <https://www.fwi.co.uk/arable/crop-management/pests/trial-shows-best-nematicide-strategy-for-pcn-in-potatoes>.
9. Dangl, J. L. & Jones, J. D. G. Plant pathogens and integrated defence responses to infection. *Nature* 2001 411:6839 411, 826–833 (2001).
10. Van Steenbrugge, J. J. M. et al. Comparative genomics of two inbred lines of the potato cyst nematode *Globodera rostochiensis* reveals disparate effector family-specific diversification patterns. doi:10.1186/s12864-021-07914-6.
11. Kochetov, A. V et al. The mechanism of potato resistance to *Globodera rostochiensis*: comparison of root transcriptomes of resistant and susceptible *Solanum phureja* genotypes. doi:10.1186/s12870-020-02334-2.

12. Scholte, K. & Vos, J. Effects of potential trap crops and planting date on soil infestation with potato cyst nematodes and root-knot nematodes. *Ann. appl. Biol* **137**, 1–53 (2000).
13. Rojas-Sandoval, J. *Solanum sisymbriifolium* (sticky nightshade). *CABI Compendium* (2020).
14. Hanuman Mhatre, P., Watpade, S., Bairwa, A. & Patil, J. Management of potato cyst nematodes with special focus on biological control and trap cropping strategies. (2022) doi:10.1002/ps.7022.
15. Trudgill, D., Phillips, M., Elliott, M. & Phillips, C. M. Dynamics and management of the white potato cyst nematode *Globodera pallida* in commercial potato crops. *Ann Appl Biol* **164**, 18–34 (2014).
16. Lambert, K. & Bekal, S. Introduction to Plant-Parasitic Nematodes. *The Plant Health Instructor* (2002) doi:10.1094/PHI-I-2002-1218-01.
17. Clarke, A. J. , S. A. M. Zinc and Other Metallic Ions as Hatching Agents for the Beet Cyst Nematode, *Heterodera schachtii* Schm. *Nature* **208**, (1965).
18. Haegeman, A., Mantelin, S., Jones, J. T. & Gheysen, G. Functional roles of effectors of plant-parasitic nematodes. (2011) doi:10.1016/j.gene.2011.10.040.
19. Hogenhout, S. A., Van Der Hoorn, R. A. L., Terauchi, R. & Kamoun, S. Emerging Concepts in Effector Biology of Plant-Associated Organisms. / *115 MPMI* **22**, 115–122 (2009).
20. Sobczak, M., Golinowski, W. & Grundler, F. M. W. Changes in the structure of *Arabidopsis thaliana* roots induced during development of males of the plant parasitic nematode *Heterodera schachtii*. *Eur J Plant Pathol* **103**, 113–124 (1997).
21. Linford, M. B. The feeding of the root-knot nematode in root tissue and nutrient solution. *Phytopathology* **27**, 824–835 (1937).
22. Wyss, U. & Zunke, U. Observations on the behaviour of second stage juveniles of Hetero inside host roots.
23. Wyss, U. & Grundler, F. M. W. Feeding behavior of sedentary plant parasitic nematodes. *Neth. J. Pl. Path* **98**, 165–173 (1992).

24. Lee, U., Chang, S., Putra, G. A., Kim, H. & Kim, D. H. An automated, high-throughput plant phenotyping system using machine learning-based plant segmentation and image analysis. (2018) doi:10.1371/journal.pone.0196615.
25. Roberts, E. H. Temperature and seed germination. *Symposia of the Society for Experimental Biology* **42**, 109–132 (1988).
26. Iyer, J., Devaul, N., Hansen, T. & Nebenfuehr, B. Chapter 25 Using Microinjection to Generate Genetically Modified *Caenorhabditis elegans* by CRISPR/Cas9 Editing. doi:10.1007/978-1-4939-8831-0\_25.
27. William Battle, M., Matthew, | & Jones, A. Cryptochromes integrate green light signals into the circadian system. (2019) doi:10.1111/pce.13643.
28. Hoson, T. Plant Growth and Morphogenesis under Different Gravity Conditions: Relevance to Plant Life in Space. *Life* **4**, 205–216 (2014).
29. The effect of gravity and centrifugal force on plants | PHYWE.  
[https://www.phywe.com/experiments-sets/university-experiments/the-effect-of-gravity-and-centrifugal-force-on-plants\\_9253\\_10184/](https://www.phywe.com/experiments-sets/university-experiments/the-effect-of-gravity-and-centrifugal-force-on-plants_9253_10184/).

# Appendices

All documents referenced in the appendices can be found in a Dropbox folder at this [web address](#).

## Appendix - Engineering methods

This section contains additional information on the design and fabrication of the imaging device, all files are found in the subfolder named ‘Engineering Methods’.

### 3D CAD design

All 3D models can be accessed found in the folder named ‘3DCAD’.

### Bill of materials

The bill of materials can be accessed in the folder named ‘BillOfMaterials’.

### I2C interface

A diagram outlining the slipring I2C interface can be found in the folder named ‘I2C’.

### Circuit diagram and PCB design

Circuit diagrams and PCB CAD files can be accessed in the folder named ‘PCB’.

### Device Python script

All Python code used by the imaging device can be found in the folder named ‘PythonDevice’.

## Appendix – data analysis

This section contains additional information on the analysis of the images, all files are found in the subfolder named ‘Data Analysis’.

### Image processing Python script

All Python code used in the image processing pipeline can be found in the folder named ‘PythonAnalysis’.

### RGB colour space

Examples of ineffective RGB data extraction graphs can be found in the folder named ‘GraphsRGB’.